

Importance of ligands in the electronic properties of $\text{FeTe}_{0.6}\text{Se}_{0.4}$

Ganesh Adhikary,¹ Deepnarayan Biswas,¹ Nishaina Sahadev,¹ Swetarekha Ram,² V. Kanchana,² C. S. Yadav,¹ P. L. Paulose,¹ and Kalobaran Maiti^{1,11}

¹Department of Condensed Matter Physics and Materials Science, Tata Institute of Fundamental Research, Homi Bhabha Road, Colaba, Mumbai - 400 005, INDIA.

²Department of Physics, Indian Institute of Technology Hyderabad, Ordnance Factory Estate, Yedumailaram, 502205, Andhra Pradesh, India

(Dated: 6 February 2019)

We investigate the electronic structure of $\text{FeTe}_{0.6}\text{Se}_{0.4}$ employing high resolution photoemission spectroscopy and *ab initio* band structure calculations. Fe 2p core level and the valence band spectra exhibit signature of strong electron correlation in the electronic structure. The electronic states near the Fermi level reduces in intensity with the decrease in temperature in conformity with the insulating transport observed near 300 K. An insulator to metal transition around 150 K could be related to the spectral lineshape change in the vicinity of the Fermi level. The spectral features near Fermi level exhibit significant *p* orbital character due to the correlation induced Fe *d* spectral weight transfer. The experimental spectra reveal dominant temperature dependence of the spectral functions possessing large *p*-character. While the origin of the anomalous electronic properties in the normal phase could be revealed in the electronic structure of this material, these results emphasizes the importance of ligand states in the high temperature superconductors that is important to explore such materials for various applications.

PACS numbers: 74.70.Xa, 74.25.Jb, 71.20.-b, 79.60.-i

I. INTRODUCTION

Discovery of superconductivity led to an enormous growth of research in both fundamental science and technology. While these materials are extensively used in medical, scientific and engineering tools, potential application in lossless power transmission, fast transport system etc. has been the major driving force in the search of new superconducting materials with high transition temperature. In this respect, the discovery of superconductivity in Fe-based systems^{1,2} renewed great attention due to the complex interplay of magnetism and superconductivity.³ These materials are significantly different from copper oxide superconductors.⁴ It is believed that Fe 3d states derive the exotic properties in these systems unlike cuprates, where the ligands play significant role.

Among Fe-based superconductors, Fe(TeSe) group of compounds are believed to be the most correlated ones due to their large ‘chalcogen height’⁵ (the height of the anions from the Fe-plane)⁶. These materials form in anti-PbO-type crystal structure (space group *P4/nmm*).⁷ The parent compounds, FeTe exhibits a spin density wave (SDW)-type antiferromagnetic transition at 65 K^{8,9} and FeSe is a superconductor below 8 K.^{10,11} Homovalent substitution of Te at Se-sites introduces disorder in the system that is expected to reduce the superconducting transition temperature, T_c .¹² In contrast, T_c increases in this system with the maximum T_c of 15 K for about 60% of Te concentration,¹³ where disorder is expected to be the most prominent. Excess Fe ($\text{Fe}_{1+y}\text{Te}_{1-x}\text{Se}_x$) in these materials exhibits magnetic ordering with bi-collinear commensurate/incommensurate structure that survives even in the highest T_c compound as a short range order.¹⁴ Electronic structure studies show band

narrowing and large mass enhancement due to electron correlation.^{15–18}

The normal phase (above T_c) of these compounds is complex exhibiting deviation from metallic conductivity near 300 K similar to that often observed in small gap semiconducting systems. Lowering of temperature leads to a transition to metallic conductivity around 150 K and eventually superconductivity appears below 15 K. Evidently, Fe(TeSe) exhibits plethora of complexity such as large electron correlation, curious disorder effects, complex normal phase etc. placing them in the pathway between other Fe-superconductors and cuprates. Here, we studied the electronic structure of $\text{FeTe}_{0.6}\text{Se}_{0.4}$ employing high resolution photoemission spectroscopy and band structure calculations. Our results reveal anomalous temperature evolution of the spectral function when the probing photon energy is varied that could be explained in terms of matrix element effect in photoemission and correlation induced enhanced chalcogen *p*-contributions near Fermi level. The observed change in electrical resistivity around 150 K has also been found to influence the photoemission spectra.

II. EXPERIMENT

The single crystalline sample of $\text{FeTe}_{0.6}\text{Se}_{0.4}$ ¹⁹ was grown by flux method and characterized by *x*-ray diffraction, Laue, Mössbauer and tunneling electron microscopic measurements establishing stoichiometric and homogeneous composition of the sample with no trace of additional Fe in the material. The photoemission measurements were carried out using a R4000 WAL electron analyzer from Gammadata scienta, monochromatic $\text{Al K}\alpha$ ($h\nu = 1486.6$ eV), He I ($h\nu = 21.2$ eV) and He II

($h\nu = 40.8$ eV) photon sources and an open cycle helium cryostat, LT-3M from Advanced Research Systems. The sample was cleaved at a base pressure better than 4×10^{-11} torr at each temperature just before the measurements. The energy resolutions were fixed to 2 meV, 5 meV and 350 meV for He I, He II and Al $K\alpha$ energies, respectively.

Band structure calculations were carried out using full-potential linearized augmented plane wave method using WIEN2k software.²⁰ In local density approximations (LDA), local uniform charge densities are considered to calculate the exchange correlation functionals. To improve upon this approximation, the exchange correlation is treated within the generalized gradient approximation (GGA),²¹ where the gradient terms of the electron density are added in the exchange correlation functionals. The GGA+ U method²² (U = on-site electron correlation strength) was employed for d electron interactions. The effective on-site Coulomb repulsion strength, $U_{eff} = 0 - 7$ eV ($U_{eff} = U - J$; J = Hund's exchange integral) was used to visualize the correlation induced changes in the electronic structure. $2 \times 2 \times 2$ supercell was used to generate the structure of $\text{FeSe}_{0.5}\text{Te}_{0.5}$. A $(25 \times 25 \times 7)$ k -point mesh corresponding to 364 k points in the irreducible part of the Brillouin zone in the Monkhorst-Pack²³ scheme was used during the self-consistent cycle.

III. RESULTS AND DISCUSSIONS

In Fig. 1(a), we show the Fe $2p$ core level spectra exhibiting interesting evolution with temperature and unusually large asymmetry relative to that of Fe metal.²⁴ The low energy excitations across the Fermi level in the photoemission final state lead to asymmetry in the spectral lineshape of metallic systems. However, the significantly large asymmetry in the present case requires consideration of three asymmetric features as denoted by 1, 2 and 3 in Fig. 1(a). These features can be attributed to the well screened final state (peak 1) and the other final states corresponding to different electron-hole excitations as observed in earlier studies of other related systems.²⁵ While the peak 1 is distinctly visible due to better energy resolution in this study, its intensity relative to the higher binding energy features is weaker than that in Fe indicating poorer itineracy of the conduction electrons in $\text{FeTe}_{0.6}\text{Se}_{0.4}$. Interestingly, the intensity of the peak 1 increases gradually with the decrease in temperature (see Figs. 1(b) and 1(c)).

Earlier theoretical studies²⁶ based on dynamical mean field theory showed that in a strongly correlated system, the valence band spectra exhibit two features. One feature appears at the Fermi level called coherent feature, which represents the itinerant electrons. The second feature, termed as incoherent feature or lower Hubbard band, corresponds to the correlation induced localized states and appears at higher binding energy. Decrease in temperature leads to an enhancement of the coherent fea-

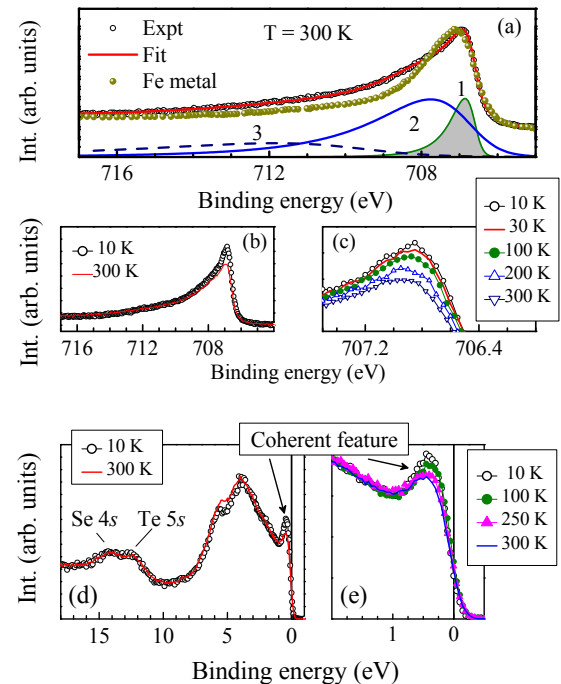


FIG. 1. (a) Fe $2p$ spectra of $\text{Fe}(\text{TeSe})$ (open circles) and Fe metal (closed circles - adapted from Ref.²⁴). Lines show the fit to the experimental spectrum. (b) Fe $2p$ spectra at 300 K and 10 K. (c) Expanded view of the temperature evolution of Fe $2p_{3/2}$ peak. (d) Valence band spectra at 300 K and 10 K. (e) Expanded view near Fermi level region.

ture intensity with a consequent decrease in the incoherent feature intensity. The valence band spectra in Figs. 1(d) and 1(e) exhibit scenario similar to the above theoretical results; the intensity near the Fermi level gradually increases with the decrease in temperature relative to the intensities at higher binding energies. This behavior of the spectral function is a manifestation of the correlation induced effect and also suggests that the intensity of itinerant electrons increases with the decrease in temperature. The enhancement of the well screened feature in the Fe $2p$ core level spectra (peak 1) with the decrease in temperature is consistent with this scenario.

In order to investigate the correlation induced effects further, the calculated electronic density of states are compared with the experimental spectra in Fig. 2. Finite electron correlation leads to a spectral weight transfer from ϵ_F to higher binding energies leading to an enhancement of intensity around 2 eV. Since the transferred spectral weight appears in the energy range similar to the energy range of bonding bands, distinct identification of the incoherent feature is non-trivial in this system. We observe that the calculated spectral functions in the whole

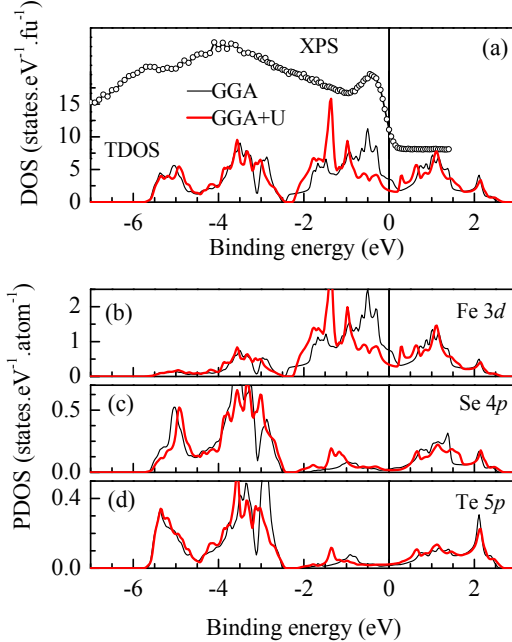


FIG. 2. (a) Calculated total density of states for uncorrelated and correlated system ($U = 4.0$ eV) and the experimental spectrum. (b) Fe 3d, (c) Se 4p and (d) Te 5p PDOS from GGA (thin line) and GGA+U (thick line) calculations with $U = 4.0$ eV.

valence band energy range with finite U exhibit better description of the experimental spectrum. For example, the calculated spectrum for $U = 4$ eV is shown in the figure providing a good description of the experimental features.

Electron correlation affects the electronic states with different orbital character differently depending on their degree of itineracy in the uncorrelated system. This is evident in Fig. 2 exhibiting significant transfer of the Fe 3d partial density of states (PDOS) to higher binding energies. Subsequently, the Se 4p / Te 5p contributions increase near ϵ_F . These results suggests strong renormalization of Fe d - chalcogen p covalency in this system.

The change in p and d contributions with the increase in U is demonstrated in Fig. 3. The electronic states near ϵ_F is primarily dominated by the Fe 3d contributions for $U = 0.0$ eV. With the increase in U , the Fe 3d partial density of states gradually shifts towards higher binding energies with substantial increase in intensity around 2 eV. Subsequently, the chalcogen p contributions near ϵ_F gradually increases making the covalent mixing much stronger compared to the uncorrelated case.

The high resolution spectra exhibit curious evolution with temperature. The He II spectra in Fig. 4(a) exhibit a broad feature near ϵ_F with no distinct change in lineshape with temperature apart from a sharp fall in intensity at ϵ_F due to the superconducting gap below T_c .²⁷

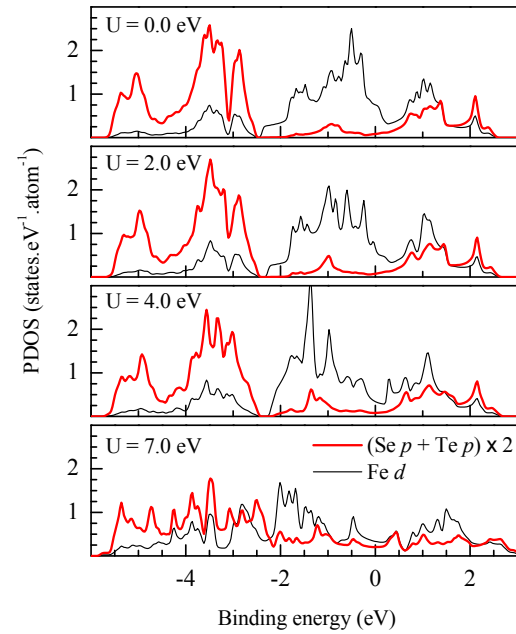


FIG. 3. Calculated partial density of states for Fe 3d and rescaled p -states [$(Te\ 5p + Se\ 4p) \times 2$] for different values of U . The contribution of p -states near the Fermi level gradually increases with respect to the Fe 3d contributions with the increase in U .

In contrast, the He I spectra exhibit two distinct features at 0.1 and 0.3 eV. The intensities of these peaks increase gradually with the decrease in temperature. Since the spectra were collected using transmission mode with a large acceptance angle of $\pm 15^\circ$, the experimental spectra will be a representation of the total density of states. Thus, the change in spectral features might have a origin different from momentum dependence. The photoemission cross section for Fe 3d states is 4.833 and 8.751 at 21.2 eV and 40.8 eV photon energies, respectively. While that of As 4p states is 3.858 and 0.2949, respectively. Thus, the relative photoemission cross-section²⁸ of As 4p to that of Fe 3d states enhances from 0.034 at 40.8 eV to 0.8 at 21.2 eV. Since the valence states are well described by the linear combination of atomic orbitals, one can conclude that the contribution of p orbital character in the conduction electronic states is significant and exhibit higher degree of sensitivity to the change in temperature.

The spectral density of states, SDOS at different temperatures are estimated by the division of the high resolution spectra by the energy resolution broadened Fermi-Dirac function. The representation of the 10 K spectra is a convolution of the above SDOS by the resolution broadened Fermi function of 10 K. Thus obtained 10 K spectra based on 300 K and 50 K spectra are compared with the raw data at 10 K in Fig. 4(b). The 300 K spectra exhibit

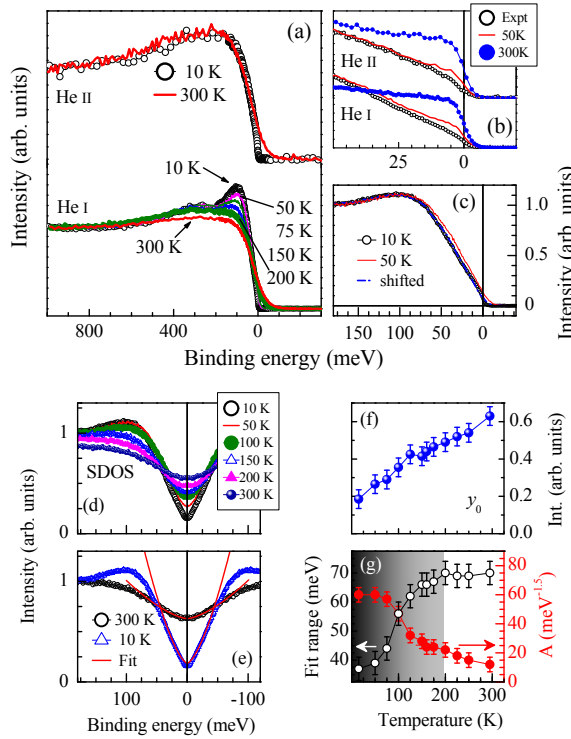


FIG. 4. (a) He I and He II spectra. (b) 10 K data (open circles) is compared with extracted 10 K spectra from 300 K (solid circles) and 50 K (line) data. (c) 50 K data (solid line) and shifted 50 K data (dashed line) are compared with 10 K data (open circles) suggesting a gap of 5 meV. (d) SDOS obtained by symmetrization at different temperature. (e) Fit for 300 K and 10 K SDOS. The fitting parameters, (f) y_0 , and (g) A & fit range.

large intensity at ϵ_F . The intensity gradually decreases with temperature as also seen in the SDOS obtained by symmetrization ($I(\epsilon) = I_0(\epsilon - \epsilon_F) + I_0(\epsilon_F - \epsilon)$) in Fig. 4(d). Such decrease in carrier concentration at ϵ_F with the decrease in temperature independent of the analysis procedure adopted might be the origin for the absence of metallic resistivity behavior near 300 K although the density of states indicate metallic phase. The photoemission spectra, however, exhibit monotonic decrease in intensity at ϵ_F with the decrease in temperature that cannot capture the transition to metallic temperature dependence of resistivity below 150 K. There are prediction of the persistence of short range antiferromagnetic order in this composition¹⁴ that might introduce such anomaly in resistivity.

In Fig. 4(c), the raw data at 50 K and 10 K are observed to be shifted due to the formation of the superconducting gap below T_c . A shift of 5 meV of the 50 K data towards higher binding energy reproduces the rising part of the spectrum at 10 K excellently well suggesting the superconducting gap of about 5 meV. The lineshape

of the spectral functions is investigated by fitting the raw data with a polynomial; the best fit is found for the relation, $I(\epsilon) = y_0 + A \times |\epsilon - \epsilon_F|^{1.5}$ as demonstrated in Fig. 4(e). The fitting parameters are shown in Figs. 4(f) and 4(g). The observed energy exponent of 1.5 indicates importance of magnetic fluctuations in the ground state.²⁹ While the fitting range starts limiting itself in the low energy regime below 150 K, coefficient, A for the spin fluctuation term starts becoming larger at the same temperature, where the transition to metallic phase occurs indicating their importance in the low temperature properties.

Effect of disorder has extensively been studied theoretically and experimentally.³⁰ Altshuler and Aronov showed that charge disorder in correlated systems exhibits $|\epsilon - \epsilon_F|^{0.5}$ dependence of the spectral lineshape near Fermi level and the spectral intensity at ϵ_F is proportional to the square root of temperature.^{31,32} In the present case, SDOS at ϵ_F , represented by y_0 in Fig. 4(f) does not follow the typical square root dependence on temperature in conformity with the above observation indicating importance of magnetic interactions in these systems.

IV. CONCLUSIONS

In summary, we studied the electronic structure of Fe-based superconductor, $\text{FeTe}_{0.6}\text{Se}_{0.4}$ employing high resolution photoemission spectroscopy and high quality single crystalline sample. The core level and valence band spectra exhibit signature of electron correlation induced features. The intensity at the Fermi level reduces gradually with the decrease in temperature suggesting decrease in conductivity as manifested by insulating temperature dependence of electronic conduction in transport measurements. The transition from insulating to metallic conductivity could be related to the change in spectral lineshape near the Fermi level.

Electron correlation renormalizes the covalency significantly leading to a significant chalcogen p orbital contributions near the Fermi level. Interestingly, the electronic spectra possessing large p character exhibit stronger sensitivity to the change in temperature. The spectral lineshape and its temperature evolution indicate importance of magnetic fluctuations in the electronic properties. Evidently, ligands play an important role in high temperature superconductivity as also found in cuprates.

V. ACKNOWLEDGEMENTS

The authors N. S. and K. M. acknowledge financial support from the Dept. of Science and Technology, Govt. of India under the Swarnajayanti fellowship programme.

¹Y. Kamihara, H. Hiramatsu, M. Hirano, R. Kawamura, H. Yanagi, T. Kamiya, and H. Hosono, J. Am. Chem. Soc. **128**, 10012 (2006).

²Y. Kamihara, T. Watanabe, M. Hirano, and H. Hosono, *J. Am. Chem. Soc.* **130**, 3296 (2008).

³N. Kurita, M. Kimata, K. Kodama, A. Harada, M. Tomita, H. S. Suzuki, T. Matsumoto, K. Murata, S. Uji, and T. Terashima, *Phys. Rev. B* **83**, 214513 (2011); G. Adhikary, N. Sahadev, D. Biswas, R. Bindu, N. Kumar, A. Thamizhavel, S. K. Dhar, and K. Maiti, *J. Phys. Condens. Matter* **25**, 225701 (2013).

⁴A. Damascelli, Z. Hussain, and Z.-X. Shen, *Rev. Mod. Phys.* **75**, 473 (2003).

⁵K. Kuroki, H. Usui, S. Onari, R. Arita, and H. Aoki, *Phys. Rev. B* **79** 224511 (2009).

⁶Y. Mizuguchi and Y. Takano, *J. Phys. Soc. Jpn.* **79**, 102001 (2010).

⁷M. Tegel, C. Löhner, and D. Johrendt, *Solid State Comm.* **150** 383 (2010).

⁸F. Ma, W. Ji, J. Hu, Z.-Y. Lu, and T. Xiang, *Phys. Rev. Lett.* **102**, 177003 (2009).

⁹A. Subedi, L. Zhang, D. J. Singh, and M. H. Du, *Phys. Rev. B* **78** 134514 (2008).

¹⁰F.-C. Hsu, J.-Y. Luo, K.-W. Yeh, T.-K. Chen, T.-W. Huang, P. M. Wu, Y.-C. Lee, Y.-L. Huang, Y.-Y. Chu, D.-C. Yan, and M.-K. Wu, *PNAS* **105** 14262 (2008).

¹¹C.-L. Song, Y.-L. Wang, P. Cheng, Y.-P. Jiang, W. Li, T. Zhang, Z. Li, K. He, L. Wang, J.-F. Jia, H.-H. Hung, C. Wu, X. Ma, X. Chen, and Q.-K. Xue, *Science* **332** 1410 (2011).

¹²A. Ghosal, M. Randeria, and N. Trivedi, *Phys. Rev. B* **65**, 014501 (2001); M. Chand, G. Saraswat, A. Kamlapure, M. Mondal, S. Kumar, J. Jesudasan, V. Bagwe, L. Benfatto, V. Tripathi, and P. Raychaudhuri, *Phys. Rev. B* **85**, 014508 (2012).

¹³C. S. Yadav, P. L. Paulose, and K. M. Subhedar, *Euro. Phys. Lett.* **90** 27011 (2010).

¹⁴W. Bao, Y. Qiu, Q. Huang, M. A. Green, P. Zajdel, M. R. Fitzsimmons, M. Zhernenkov, S. Chang, M. Fang, B. Qian, E. K. Vehstedt, J. Yang, H. M. Pham, L. Spinu, and Z. Q. Mao, *Phys. Rev. Lett.* **102**, 247001 (2009).

¹⁵K. Nakayama, T. Sato, P. Richard, T. Kawahara, Y. Sekiba, T. Qian, G. F. Chen, J. L. Luo, N. L. Wang, H. Ding, and T. Takahashi, *Phys. Rev. Lett.* **105**, 197001 (2010).

¹⁶F. Chen, B. Zhou, Y. Zhang, J. Wei, H.-W. Ou, J.-F. Zhao, C. He, Q.-Q. Ge, M. Arita, K. Shimada, H. Namatame, M. Taniguchi, Z.-Y. Lu, J. Hu, X.-Y. Cui, and D. L. Feng, *Phys. Rev. B* **81**, 014526 (2010).

¹⁷A. Tamai, A. Y. Ganin, E. Rozbicki, J. Bacsa, W. Meevasana, P. D. C. King, M. Caffio, R. Schaub, S. Margadonna, K. Prassides, M. J. Rosseinsky, and F. Baumberger, *Phys. Rev. Lett.* **104**, 097002 (2010).

¹⁸M. Aichhorn, S. Biermann, T. Miyake, A. Georges, and M. Imada, *Phys. Rev. B* **82**, 064504 (2010).

¹⁹C. S. Yadav and P. L. Paulose, *New J. Phys.* **11**, 103046 (2009).

²⁰P. Blaha, K. Schwarz, G. K. H. Madsen, D. Kvasnicka, and J. Luitz, **WIEN2k**, An Augmented Plane Wave + Local Orbitals Program for Calculating Crystal Properties (Karlheinz Schwarz, Techn. Universität Wien, Austria), 2001. ISBN 3-9501031-1-2.

²¹J. P. Perdew, K. Burke, and M. Ernzerhof, *Phys. Rev. Lett.* **77**, 3865 (1996).

²²M. T. Czyzyk and G. A. Sawatzky, *Phys. Rev. B* **49**, 14211 (1994).

²³H. J. Monkhorst and J. D. Pack, *Phys. Rev. B* **13**, 5188 (1976).

²⁴J. F. van Acker, Z. M. Stadnik, J. C. Fugle, H. J. W. M. Hoekstra, K. H. J. Buschow, and G. Stroink, *Phys. Rev. B* **37**, 6827 (1988).

²⁵M. Takahashi and J.-I. Igashiki, *Phys. Rev. B* **85**, 085128 (2012).

²⁶A. Georges, G. Kotliar, W. Krauth, and M. J. Rozenberg, *Rev. Mod. Phys.* **68**, 13 (1996); M. Imada, A. Fujimori, and Y. Tokura, *Rev. Mod. Phys.* **70**, 1039 (1998).

²⁷V. R. R. Medicherla, S. Patil, R. S. Singh, and K. Maiti, *Appl. Phys. Lett.* **90**, 062507 (2007).

²⁸J. J. Yeh and I. Lindau, *At. Data and Nucl. Data Tables* **32**, 1 (1985); K. Maiti, P. Mahadevan, and D. D. Sarma, *Phys. Rev. B* **59**, 12457 (1999); K. Maiti and D. D. Sarma, *Phys. Rev. B* **58**, 9746 (1998).

²⁹K. Maiti, R. S. Singh, V. R. R. Medicherla, S. Rayaprol, and E. V. Sampathkumaran, *Phys. Rev. Lett.* **95**, 016404 (2005); K. Maiti, R. S. Singh, and V. R. R. Medicherla, *Phys. Rev. B* **76**, 165128 (2007); R. S. Singh, V. R. R. Medicherla, K. Maiti, and E. V. Sampathkumaran, *Phys. Rev. B* **77**, 201102(R) (2008).

³⁰P. A. Lee and T. V. Ramakrishnan, *Rev. Mod. Phys.* **57**, 287 (1985).

³¹B. L. Altshuler and A. G. Aronov, *Solid State Commun.* **30**, 115 (1979).

³²M. Kobayashi, K. Tanaka, A. Fujimori, S. Ray, and D. D. Sarma, *Phys. Rev. Lett.* **98**, 246401 (2007); K. Maiti, R. S. Singh, and V. R. R. Medicherla, *Europhys. Letts.*, **78**, 17002 (2007); *ibid.*, *Phys. Rev. B* **76**, 165128 (2007).